bioRxiv preprint doi: https://doi.org/10.1101/2020.02.26.962753; this version posted February 26, 2020. The copyright holder for this preprint (which was not certified by peer review) is the author/funder, who has granted bioRxiv a license to display the preprint in perpetuity. It is made available under aCC-BY-NC-ND 4.0 International license.

1
2
3 # Suppression of Inflammation Delays Hair Cell Regeneration and Functional Recovery Following Lateral Line Damage in Zebrafish Larvae

4 Ru Zhang[2,3], Xiao-Peng Liu[3,4], Ya-Juan Li[2], Ming Wang[1,3], Lin Chen[1,3*],
5 Bing Hu[1,2*]
6
7 1 CAS Key Laboratory of Brain Function and Diseases, School of Life
8 Sciences, University of Science and Technology of China, Hefei 230027,
9 China.
10 2 Lab of Neurodevelopment and Repair, University of Science and
11 Technology of China, Hefei 230027, China.
12 3 Auditory Research Laboratory, University of Science and Technology of
13 China, Hefei 230027, China.
14 4 Center for Hearing and Deafness, State University of New York at Buffalo,
15 NY14214, USA.
16
17
18
19 **[*]Corresponding authors.**
20 Bing Hu, PhD, Lab of Neurodevelopment and Repair, University of Science
21 and Technology of China, Hefei 230027, China.
22 Tel.: +86 (551) 6360-2489
23 E-mail: bhu@ustc.edu.cn
24 Lin Chen, PhD, Auditory Research Laboratory, University of Science and
25 Technology of China, Hefei 230027, China.
26 Tel.: +86 (551) 6360-7623
27 E-mail: linchen@ustc.edu.cn
28

bioRxiv preprint doi: https://doi.org/10.1101/2020.02.26.962753; this version posted February 26, 2020. The copyright holder for this preprint (which was not certified by peer review) is the author/funder, who has granted bioRxiv a license to display the preprint in perpetuity. It is made available under aCC-BY-NC-ND 4.0 International license.

Abstract:

Background: Human cochlear hair cells cannot regenerate after loss. In contrast, those in fish and amphibians have a remarkable ability to regenerate after damaged. Previous studies focus on mechanisms of hair cell regeneration, such as Wnt and Notch signals. These studies ignore the fact that the beginning of regeneration is accompanied by a large number of inflammatory responses. The role of this inflammation in hair cell regeneration is still unknown. In addition, there is no appropriate behavioral method to quantitatively evaluate the functional recovery of lateral line hair cells after regeneration.

Results: In this study, we found that when inflammation was suppressed, the regeneration of lateral line hair cells and the recovery of the rheotaxis of the larvae were significantly delayed. Calcium imaging showed that the function of the neuromasts in the inflammation-inhibited group was weaker than that in the non-inflammation-inhibited group at the Early Stage of regeneration, and returned to normal at the Late Stage. Calcium imaging also revealed the cause of the mismatch between the function and quantity during regeneration.

Conclusions: Our results, meanwhile, suggest that suppressing inflammation delays hair cell regeneration and functional recovery when hair cells are damaged. This study may provide a new idea for how to promote hair cell regeneration and functional recovery in adult mammals.

Keywords: inflammation, hair cell regeneration, neuromast, lateral line, zebrafish larva, rheotaxis, calcium imaging.

bioRxiv preprint doi: https://doi.org/10.1101/2020.02.26.962753; this version posted February 26, 2020. The copyright holder for this preprint (which was not certified by peer review) is the author/funder, who has granted bioRxiv a license to display the preprint in perpetuity. It is made available under aCC-BY-NC-ND 4.0 International license.

56 ## Background:

57 Deafness and hearing defects are usually caused by loss of sensory hair
58 cells or defect of auditory function. The loss of hair cells is result of aging,
59 infection, genetic factors, hypoxia, autoimmune disorder, ototoxic drugs or
60 noise exposure. Unfortunately, including humans, hair cells cannot regenerate
61 in mammals (Oesterle and Stone, 2008; Yorgason. et al., 2006). In contrast,
62 hair cells in some non-mammalian vertebrates have a remarkable ability to
63 regenerate, such as birds, reptiles, amphibians and fish (Matsui. and
64 Cotanchea., 2004; Popper and Hoxter, 1984; Stone. and Rubel., 2000). It
65 could suggest that if we figure out the mechanism of hair cell regeneration in
66 these species, we probably can promote hair cell regeneration in mammals.

67 When hair cells are damaged, support cells proliferate into both hair cells
68 and support cells, or convert into hair cells directly(Baird et al., 1996;
69 Lopez-Schier and Hudspeth, 2006; Raphael, 1992; Roberson et al., 2004).
70 Hair cell regeneration is finely regulated by the interaction of multiple signaling
71 pathways, such as Notch signaling(Ma et al., 2008; Mizutari et al., 2013),
72 Wnt/b-catenin signaling(Aman and Piotrowski, 2008; Chai et al., 2012; Shimizu
73 et al., 2012), Fgf signaling(Aman and Piotrowski, 2008; Nechiporuk and Raible,
74 2008), retinoic acid(Rubbini et al., 2015) and so on. In the process of hair cell
75 damaged, it is accompanied by a lot of inflammatory reaction, which has been
76 found to play a role in tissue regeneration in recent years(Mescher, 2017). For
77 example, macrophages are considered having main function in the
78 inflammatory resolution stage and being required for fin regeneration(Li et al.,
79 2012) and hair cell regeneration in zebrafish(Carrillo et al., 2016). In addition, it
80 has been confirmed that neutrophils in mice play a central role in
81 inflammation-induced optic nerve regeneration(Kurimoto et al., 2013).

82 In recent years, zebrafish (Danio rerio) has become an ideal model for
83 studying inflammation and hair cell regeneration because it has conservative

bioRxiv preprint doi: https://doi.org/10.1101/2020.02.26.962753; this version posted February 26, 2020. The copyright holder for this preprint (which was not certified by peer review) is the author/funder, who has granted bioRxiv a license to display the preprint in perpetuity. It is made available under aCC-BY-NC-ND 4.0 International license.

84 innate immunity (Renshaw and Trede, 2012) and strong regeneration ability in
85 lateral line system(Lush and Piotrowski, 2014) which makes zebrafish larvae
86 to perceive the change of surrounding flow, detect their prey and avoid
87 predators(Coombs. et al., 2014; Dijkgraaf, 1962). The lateral system of a larva
88 is composed of neuromasts which located on the surface of the body.
89 The neuromasts on the head consist of the anterior lateral line system (aLL)
90 and the ones along the body comprise the posterior lateral line system
91 (pLL)(Thomas et al., 2015). The center of the neuromast is composed of hair
92 cells and they are surrounded by support cells and mantle cells. At the top of
93 the hair cells, rows of short stereocilia and a long kinocilium extend out of the
94 body called the hair bundle and are covered in a gelatinous cupula. The
95 arrangement of stereocilia and kinocilium determines the polarity of hair cells
96 and the polarity of the hair cells is planar cell polarity (PCP), which is arranged
97 symmetrically (Flock and Wersall, 1962), half in each direction.

98 When hair bundles are deflected, hair cells release transmitters and cause
99 exciting spikes in afferent neurons(Dijkgraaf, 1962). And then, larvae show a
100 robust behavior called rheotaxis(Olszewski et al., 2012). This behavior can be
101 applied to evaluate the function of hair cells (Suli et al., 2012).

102 In recent years, calcium imaging has become a popular method to
103 measure the function of neural cells in detail and quantitatively (Zhang et al.,
104 2016). When the mechanical hair bundle deflected, calcium and other cations
105 enter into cytoplasm through mechanotransduction channels. It changes the
106 membrane potential and activates voltage-gated calcium channels which allow
107 rapid calcium inflow to trigger synaptic transmission. GCaMPs, a
108 genetically-encoded calcium indicator(GECIs), are single fluorescent proteins,
109 which can bind calcium directly and alter conformation to respond the change
110 of calcium concentration(Tian et al., 2012). These significant,
111 activity-dependent signals can reflect the function of hair cells in a single

bioRxiv preprint doi: https://doi.org/10.1101/2020.02.26.962753; this version posted February 26, 2020. The copyright holder for this preprint (which was not certified by peer review) is the author/funder, who has granted bioRxiv a license to display the preprint in perpetuity. It is made available under aCC-BY-NC-ND 4.0 International license.

112 neuromast (Zhang et al., 2018; Zhang et al., 2016).

113 Previous research has found that the deletion of macrophages by
114 morpholino leads to the delay of hair cell regeneration(Carrillo et al., 2016).
115 However, does it still cause the delay of hair cell regeneration when the
116 macrophages are intact, and the pro-inflammatory factors are suppressed as
117 the hair cells are damaged? Is there any delay in the functional recovery of the
118 lateral line?

119 In order to figure out the above problems, we used an anti-inflammatory
120 agent, BRS-28, to suppress the inflammation when hair cells are damaged by
121 copper. BRS-28 is a derivative of 5α-cholestan-6-one, which was confirmed to
122 be a remarkably suppressor of the production of pro-inflammatory factors,
123 such as NO, TNF-α、IL-1β、iNOS and cox-2(Yang et al., 2014). We count the
124 number of neutrophils and macrophages in Tg(corola-eGFP; lyz-Dsred)
125 transgenic line. Then, AB/WT zebrafish larvae were used to count the number
126 of regenerated hair cells. Since there is no appropriate behavioral method to
127 quantitatively evaluate the function of lateral line hair cells, we designed and
128 built devices to test rheotaxis behavior in AB/WT larvae. A behavioral analysis
129 software was applied for quantitative evaluation of rheotaxis, so as to reflect
130 the holistic functional recovery of the posterior lateral line. Finally, the function
131 of the regenerated hair cells in a single neuromast was evaluated by the
132 method of calcium imaging in Huc:h2b-gcamp6f transgenic line.

133

134 Results

135 $CuSO_4$ damaged hair cells in lateral line of zebrafish.

136 Sensory hair cells in a 6-day post fertilization (dpf) AB/WT zebrafish larva
137 were labeled with 0.05% DASPEI clearly (**Fig. 1A**). L2、LII2、L3 neuromasts
138 (circles in **Fig.1 A**) were three of the posterior lateral neuromasts, which

bioRxiv preprint doi: https://doi.org/10.1101/2020.02.26.962753; this version posted February 26, 2020. The copyright holder for this preprint (which was not certified by peer review) is the author/funder, who has granted bioRxiv a license to display the preprint in perpetuity. It is made available under aCC-BY-NC-ND 4.0 International license.

139 located along the flat truck body and easily to be observed. A lateral view of the
140 neuromasts showed the elongated kinocilia extending from the body (**Fig. 1B**).
141 The neuromasts are consisted of hair cells surrounded by support cells, which
142 are surrounded by mantle cells (**Fig. 1C**). In order to study the effects of
143 inflammation on hair cell regeneration, we established a hair-cell-damaged
144 model. Hair cells were damaged completely, when treated with 5 μM $CuSO_4$
145 for 1 h (**Fig. 1D**). Labeled with 0.05% DASPEI, hair cells displayed close
146 arrangement and clear boundary. Only treated with $CuSO_4$ solution for 20 min,
147 hair cells became loose and unclear which suggested that they were already
148 injured. The number of hair cells decreased with weaker fluorescence intensity
149 and obscure cell boundary at 40 min. Hair cells were completely disappeared
150 at 60 min, indicating that they had been completely damaged. TUNEL assay
151 revealed the missing hair cells underwent apoptosis (**Supplementary Fig. 1**).
152 After being transferred to embryo medium (EM), the number of hair cells
153 quickly returned to normal (**Fig. 1E**).

154 **BRS-28 reduced the number of neutrophils and macrophages migrating**
155 **to the injured neuromasts.**

156 Neutrophils (**Fig. 2B, C**, blue arrows) and macrophages (**Fig. 2B, C**, white
157 arrows) could be marked and distinguished in larvae of Tg(corola-eGFP;
158 lyz-Dsred) transgenic line (**Supplementary Fig. 2**). Normally, neutrophils and
159 macrophages were almost absent from the neuromasts (example, **Fig. 2A**).
160 When treated with $CuSO_4$ solution, hair cells were damaged. Neutrophils and
161 macrophages migrated to neuromasts within 1 hours (example, **Fig. 2B**).
162 When larvae were immerged in BRS-28, an anti-inflammatory agent, before
163 treated with $CuSO_4$ solution, less neutrophils and macrophages migrated to
164 the damaged neuromasts (example, **Fig. 2C**). When the inflammation
165 suppressed, the numbers of neutrophils appeared around the damaged
166 neuromasts were lower at 0.5,1,3 and 4 h after add the $CuSO_4$ solution in

bioRxiv preprint doi: https://doi.org/10.1101/2020.02.26.962753; this version posted February 26, 2020. The copyright holder for this preprint (which was not certified by peer review) is the author/funder, who has granted bioRxiv a license to display the preprint in perpetuity. It is made available under aCC-BY-NC-ND 4.0 International license.

167 BRS+$CuSO_4$ group than in $CuSO_4$ group (**Fig. 2D**). In addition, we observed
168 BRS+$CuSO_4$ group had fewer macrophages at 0.5, 1, 2 and 3 h than $CuSO_4$
169 group (**Fig. 2E**). Collectively, the data strongly suggested that BRS-28 reduced
170 the number of neutrophils and macrophages migrating to the injured
171 neuromasts. It was worth noting that compared with control, there was no
172 significant difference in the numbers of neutrophils and macrophages between
173 $CuSO_4$ group and BRS+$CuSO_4$ group at 5 and 6 h, indicating that the
174 inflammation was resolved.

175 **Suppressing inflammation delayed hair cell regeneration.**

176 In order to investigate whether the regeneration of hair cells were delayed
177 after suppressing inflammation, we observed hair cells in the L2, LII2 and L3
178 neuromasts. We found that the regeneration of hair cells was delayed after the
179 inflammation was suppressed by the inflammatory inhibitor, BRS-28. Live
180 imaging showed regenerated hair cells in $CuSO_4$, BRS+$CuSO_4$ group at 24, 48
181 and 96 hours post injured (hpi) by $CuSO_4$(**Fig. 3A**). Control group was showed
182 at the same time point. Further analysis revealed that the numbers of
183 regenerated hair cells were significantly decreased in BRS+$CuSO_4$ group than
184 that in $CuSO_4$ group at 16 hpi ($P=0.0061$), 24 hpi ($P=0.0021$) and 48 hpi
185 ($P<0.0001$) (**Fig. 3B**, n = 30 neuromasts). These results indicated that the
186 regeneration of hair cells was delayed in BRS+$CuSO_4$ group within 48 hpi.
187 Compared with Control group, there was no difference in the number of hair
188 cells between $CuSO_4$ group and BRS+$CuSO_4$ group at 96 hpi, suggesting that
189 hair cells were regenerated to the normal level at 96 hpi. We also analyzed the
190 number of hair cells when only teated with BRS-28 (BRS group). As expected,
191 BRS group had no difference with Control group at any time point, excluding
192 the effect of BRS-28 on hair cells.

193 Since hair cells did not regenerate at a uniform rate, we defined the time
194 of regeneration into two periods: the Early Stage which includes the time from

bioRxiv preprint doi: https://doi.org/10.1101/2020.02.26.962753; this version posted February 26, 2020. The copyright holder for this preprint (which was not certified by peer review) is the author/funder, who has granted bioRxiv a license to display the preprint in perpetuity. It is made available under aCC-BY-NC-ND 4.0 International license.

195 0 to 48 hpi and the Late Stage which includes the time after 48 hpi. The
196 regeneration of hair cells was fast in the Early Stage and slow in the Late Stage.
197 Linear analysis was conducted on the number of hair cell regeneration in the
198 Early Stage. The slope in $CuSO_4$ group (0.1879) was higher than that in
199 BRS+$CuSO_4$ group (0.148) , meanwhile, x-intercept in $CuSO_4$ group (4.16)
200 was higher than that in BRS+$CuSO_4$ group (8.287) (**Fig. 3C, D**). These implied
201 that the hair cell regeneration in BRS+$CuSO_4$ group may begin later and
202 slower than that in $CuSO_4$ group.

203 To explore whether the time window of inflammatory suppression had
204 contribute to delayed regeneration, we changed the start time of BRS-28
205 treatment. We found that compared with the $CuSO_4$ group, whether BRS-28
206 was added at the same time as $CuSO_4$ ($CuSO_4$+BRS 0 h group), or 30 minutes
207 after the addition of $CuSO_4$ ($CuSO_4$+BRS 0.5 h group), or 1 hour after the
208 addition of $CuSO_4$($CuSO_4$+BRS 1 h group) (**Fig. 3E**), there was no statistical
209 difference on the number of regenerated hair cells.

210 To sum up, the regeneration of hair cells in lateral line was delayed after
211 the inflammation was suppressed by the inflammatory inhibitor BRS-28.

212 **The functional recovery of the lateral line system was delayed when**
213 **inflammation was suppressed.**

214 Since the rheotaxis could reflect the function of the lateral line, we
215 designed a behavioral device to test the rheotaxis of zebrafish (**Fig. 4A**, see
216 details in Materials and Methods). Larvae were placed from the right platform,
217 and they sense the water flow from right to left. **Figure 4B, C** were two
218 examples of larval rheotaxis processed by behavioral analysis software: the
219 former was a larva with excellent rheotaxis(**Fig. 4B**) and the latter was a larva
220 performed failure in the rheotaxis test(**Fig. 4C**). The left panels in these two
221 examples showed the track of this larva. The behavioral analysis software
222 mapped the movement path of larvae by line segment. The color of the line

bioRxiv preprint doi: https://doi.org/10.1101/2020.02.26.962753; this version posted February 26, 2020. The copyright holder for this preprint (which was not certified by peer review) is the author/funder, who has granted bioRxiv a license to display the preprint in perpetuity. It is made available under aCC-BY-NC-ND 4.0 International license.

223 segment represented the direction of movement of the larvae. All the
224 movements from right to left were represented by purplish or red segments,
225 where purple indicated that the velocity along the flow direction was greater
226 than or equal to the flow velocity, and red indicated that the velocity along the
227 flow direction was less than the flow velocity. All the movements from left to
228 right were represented by green segments, and the higher the brightness was,
229 the faster the speed was. The right panels displayed the motion vector. The
230 lengths of the blue segments represented the distance of each movement, and
231 the direction of the blue segment represented the direction of that movement.
232 The length of the red line segment was the ratio of motion vectors sum to the
233 motion arithmetic sum and the direction was the direction of the sum of the
234 vectors.

235 When the red segment was long and had a small angle of 0 degree, it
236 indicated that the motion of the larva was consistent with the opposite direction
237 of flow. It represented that the larva had good rheotaxis, indicating its lateral
238 line system had good function. Therefore, the software reported a high score.
239 On the contrary, when the red segment was short or had a small angle of 180
240 degree, it indicated that the larva moved randomly and had a poor rheotaxis,
241 indicating its lateral line system had poor function. In this case, the software
242 reported a low score. The scores reported by the software were plotted into bar
243 charts and showed in **Figure 4D**. After the hair cells were damaged by $CuSO_4$,
244 there was little rheotaxis in both $CuSO_4$ group and BRS+$CuSO_4$ group. At 24
245 and 48 hpi, the rheotaxis of BRS+$CuSO_4$ group was significantly lower than
246 that of control. On the contrary, the rheotaxis of $CuSO_4$ group was not
247 significantly different from that of control within 24 hpi. Therefore, it indicated
248 that the functional recovery of lateral line system was delayed in BRS+$CuSO_4$
249 group. The rheotaxis of BRS group at each time point was not different from
250 that of control, suggesting that BRS-28 had no significant effect on the

bioRxiv preprint doi: https://doi.org/10.1101/2020.02.26.962753; this version posted February 26, 2020. The copyright holder for this preprint (which was not certified by peer review) is the author/funder, who has granted bioRxiv a license to display the preprint in perpetuity. It is made available under aCC-BY-NC-ND 4.0 International license.

251 rheotaxis. In addition, we noted that the speed and distance of each
252 movements were consistent within different times and between different
253 groups: both were stable at around 22 mm/s (**Fig. 4E, F**), which indicated that
254 BRS-28 or $CuSO_4$ did not affect the movement of zebrafish.

255 The conclusion was that the regenerated hair cells still had the ability to
256 sense water flow, but the functional recovery of lateral line system was delayed
257 when inflammation was suppressed.

258 **Calcium imaging revealed the function of a single neuromast after hair**
259 **cell regeneration**

260 Since we found a mismatch between the function of the lateral line and the
261 amount of hair cell regeneration, that is, after the zebrafish lateral line was
262 damaged by copper sulfate, it took 96 h for the hair cells to return to normal,
263 while the flow ability returned to normal at 24 h. The function of a single
264 neuromast can be evaluated by observing its calcium activity (Zhang et al.,
265 2016). The L3 neuromast, located in flat trunk, was stimulated by water flow
266 from an electrode (**Fig. 5A**). Since hair cells had polarities, the yellow and
267 green hair cells represented opposite polarities. Chou et al. reported that the
268 polarity of the L3 neuromast is parallel to the anterior-posterior body axis(Chou
269 et al., 2017). Thus, by adjusting the direction of the electrode, water was
270 controlled to flow in two directions: anterior to posterior (A-P) direction or
271 posterior to anterior (P-A) direction. We found that not all hair cells responded
272 to the water flow, and only some hair cells were active (example, **Fig. 5B**,
273 circled cells). These active cells only responded to stimulus in one direction:
274 P-A direction (**Fig. 5C**, yellow ones and yellow circles in **Fig. 5B**) or A–P
275 direction (**Fig. 5D**, green ones and green circles in **Fig. 5B**). Because the
276 neuromasts were stereoscopic, some of the active hair cells were far from this
277 focal plane (dashed circles in **Fig. 5B**) and were not included in subsequent
278 fluorescence intensity analysis.

bioRxiv preprint doi: https://doi.org/10.1101/2020.02.26.962753; this version posted February 26, 2020. The copyright holder for this preprint (which was not certified by peer review) is the author/funder, who has granted bioRxiv a license to display the preprint in perpetuity. It is made available under aCC-BY-NC-ND 4.0 International license.

279 Similar to the results of the rheotaxis, the fluorescence intensity(ΔF/F) of
280 the regenerated hair cells were reduced significantly when inflammation was
281 suppressed at the Early Stage of regeneration (within 48 hpi)(**Fig. 5E**). It was
282 noteworthy that compared to control group, the fluorescence intensity in
283 $CuSO_4$ group did not decrease significantly in the Early Stage of regeneration.
284 This might explain that why the rheotaxis in $CuSO_4$ group had been recovered
285 at 24 hpi. The fluorescence intensity of BRS+$CuSO_4$ group was not
286 significantly different from that of control group and $CuSO_4$ group in the Late
287 Stage of regeneration (72-96 hpi) (**Fig. 5F**). Additionally, the fluorescence
288 intensity showed no differences between BRS group and control group (**Fig.
289 5G**), indicating that BRS-28 had no effect on the fluorescence intensity.

290 Normally, only a part of the hair cells in the neuromast responds to the
291 stimulation of water flow. Is it the same for regenerated hair cells? We found
292 that only a few regenerated hair cells in $CuSO_4$ group and BRS+$CuSO_4$ group
293 responded to flow stimuli. The number of active cells in each neuromast in
294 these two group were approximately the same at 24 to 96 hpi, and were
295 consistent with that in control group (**Fig. 5H**).

296 Furthermore, we noticed that most hair cells that responded to the flow in
297 the opposite direction came in pairs (**Supplementary Fig. 3A**). Although the
298 numbers of hair cells responding to flow in P-A direction were similar to that in
299 A-P direction, the fluorescence intensity of hair cells responding to P-A
300 direction was significantly higher than that of hair cells responding to A-P
301 direction (**Supplementary Fig. 3B**). It indicated that L3 neuromast was more
302 sensitive to the flow from the P-A direction.

303 The results demonstrated that the recovery of hair cell function was
304 delayed at the Early Stage of regeneration when inflammation was
305 suppressed.

306

bioRxiv preprint doi: https://doi.org/10.1101/2020.02.26.962753; this version posted February 26, 2020. The copyright holder for this preprint (which was not certified by peer review) is the author/funder, who has granted bioRxiv a license to display the preprint in perpetuity. It is made available under aCC-BY-NC-ND 4.0 International license.

307 # Discussion

308 **BRS-28 suppresses inflammation and delays the initiation of hair cell**
309 **regeneration.**

310 Although the downregulation of Notch signal during lateral line
311 regeneration induces the proliferation of support cells by activating
312 Wnt/b-Catenin signal (Romero-Carvajal et al., 2015), it is still unknown how the
313 downregulation of Notch signal is triggered after the death of hair cells. Kniss
314 and his colleague proposed a hypothesis of triggering hair cell regeneration in
315 2016 (Kniss et al., 2016). They believed that apoptosis initiated the
316 proliferation of peripheral cells to promote tissue repair (Fan and Bergmann,
317 2008; Mollereau et al., 2013) and they called this process as compensatory
318 proliferation. They assumed that a similar process may be involved in the
319 regeneration of hair cells. On the basis of their hypothesis , we speculate that
320 when hair cells are damaged by $CuSO_4$, it cause apoptosis in lateral line hair
321 cells, trigger the rise of reactive oxygen species (ROS) and reactive nitrogen
322 species (RNS), and induce the oxidative stress. This process may improve
323 AP-1,HIF-1α and NF-κB activity, and thus increase pro-inflammatory cytokines
324 and chemokines, such as NO, IL-1β, TNF-α, cox-2,iNOS and so on (Pereira et
325 al., 2016). BRS-28, suppress the production of NO、IL-1β、TNF-α、cox-2、iNOS
326 (Yang et al., 2014), reducing the number of neutrophils and macrophages
327 migrating to the damage of neuromasts. Besides that, the decrease of
328 pro-inflammatory factors may reduce the activation of macrophages. These
329 processes would decrease the production of TNF ligands and inhibit the JNK
330 signal, which contributes to initiating cells regeneration, and eventually leads
331 to delay initiation of compensatory proliferation and delay regeneration of hair
332 cells.

333 When the initiate time of inflammatory inhibitors changed, there is no
334 delay in the amount of regeneration. This also suggests that the timing of

bioRxiv preprint doi: https://doi.org/10.1101/2020.02.26.962753; this version posted February 26, 2020. The copyright holder for this preprint (which was not certified by peer review) is the author/funder, who has granted bioRxiv a license to display the preprint in perpetuity. It is made available under aCC-BY-NC-ND 4.0 International license.

335 inflammation suppression is important: when inflammation occurs,
336 compensated proliferation of the support cells has been triggered and hair cell
337 regeneration has been initiated. If inflammation suppression does not take
338 effect, regeneration seems to be unaffected.
339 In addition, neutrophils can also remove dead cell debris, and
340 macrophages can absorb apoptotic neutrophils or fragments of dead cells. We
341 suggest that neutrophils and macrophages with reduced number and activity
342 become slow in cleaning up damaged tissue areas, so as to have a good
343 regeneration environment. Since the damaged neuromasts need more time to
344 clean up these cell fragments, it may also delay the regeneration of hair cells.
345 **Suppression of inflammation delays functional recovery of regenerated**
346 **hair cells**
347 In this study, we have found that the number of hair cells decreased when
348 inflammation was suppressed which is the same as the functional recovery.
349 Finally, the quantity and the function of hair cells will be consistent with the
350 recovery of the normal level. Therefore, although the suppression of
351 inflammation delayed the regeneration of hair cells, it did not affect the overall
352 process of hair cell regeneration, and the function of hair cells regenerated in
353 the state of low inflammation eventually tended to be intact. These phenomena
354 are also consistent with the hypothesis I mentioned earlier. However, the effect
355 of inflammation on the regeneration of lateral hair cells seems to be different
356 from that of the fin. In 2012, Li and his colleague found that when zebrafish
357 larvae lacked macrophages, vacuoles appeared in the regenerated fin, which
358 suggests that macrophages may also be involved in the regeneration of the fin.
359 In our research, although the suppression of inflammation has delayed hair cell
360 regeneration and its recovery of function at the Early Stage of regeneration,
361 they eventually return to the normal status at the Late Stage of regeneration.
362 This is not because inflammation is not suppressed sufficiently, as Carrillo et al.

bioRxiv preprint doi: https://doi.org/10.1101/2020.02.26.962753; this version posted February 26, 2020. The copyright holder for this preprint (which was not certified by peer review) is the author/funder, who has granted bioRxiv a license to display the preprint in perpetuity. It is made available under aCC-BY-NC-ND 4.0 International license.

363 found in their study that the number of hair cells finally completed regeneration
364 even when macrophages was knockout(Carrillo et al., 2016). But that, this may
365 be because the injured organs are different, and the intact function of lateral
366 hair cells is crucial for the survival of zebrafish. We suggest that the hair cells
367 in lateral line may have more complex regulation in regeneration.

368 **The functional recovery of hair cells is much faster than its quantity**

369 Previous studies have focused on the morphological and quantitative
370 recovery of regenerated hair cells in zebrafish (Carrillo et al., 2016;
371 Romero-Carvajal et al., 2015). Since the regeneration takes 3-4 days post
372 injured, it is easy to assume that the recovery of the function of the neuromasts
373 may be proportional to the number of regenerated hair cells. In this study, for
374 the first time, we performed a method for evaluating the function of
375 regenerated hair cells. We found that the $CuSO_4$ group already performed
376 excellent rheotaxis at 24 hpi (Fig. 4 C), although the average number of hair
377 cells was only 3.667 at that time (Fig. 3 B). Thus, the functional recovery of hair
378 cells is much faster than its quantity. In other words, although it takes 72-96 h
379 to complete regeneration, the function of hair cells can be recovered at 24 h. It
380 is critical to the survival of zebrafish. When BRS-28 is used to suppress the
381 inflammation, the amplitude of calcium activity of hair cells was significantly
382 lower than not only that of control group but that of $CuSO_4$ group which makes
383 larvae show poor rheotaxis at the Early Stage of regeneration. Therefore, the
384 suppression of inflammation not only delays the hair cell regeneration, but also
385 delays the functional recovery.

386 We noticed that there is a mismatch between the function and quantity
387 during regeneration. Calcium image has revealed that only a part of hair cells
388 in one neuromast respond to the flow. This result is consistent with previous
389 study(Zhang et al., 2018). We have found that this phenomenon also exists in
390 regeneration group ($CuSO_4$ and BRS+$CuSO_4$ group). No matter what the

bioRxiv preprint doi: https://doi.org/10.1101/2020.02.26.962753; this version posted February 26, 2020. The copyright holder for this preprint (which was not certified by peer review) is the author/funder, who has granted bioRxiv a license to display the preprint in perpetuity. It is made available under aCC-BY-NC-ND 4.0 International license.

391 amount of regenerated hair cells is, the number of hair cells responding to the
392 flow remained stable during regeneration and has no differences with that of
393 the controls (Fig5 H). Besides that, the magnitude of fluorescence intensity
394 and reaction time is also consistent with that of the controls. This explains
395 why the number of regeneration in the $CuSO_4$ group at 24 h is only 3.667 on
396 average, but the function of the lateral line has been restored to the level very
397 close to that of the control group.

398 In this study, We only performed calcium imaging on the L3 neuromast,
399 which was confirmed as the polarity of the A-P body axis in the study of Chou
400 et al(Chou et al., 2017). Consistent with their results, we also found this
401 neuromast is insensitive to the flow in the dorsal-ventral (D-V) body axis.
402 Therefore, this study only focused on the stimulus response in the direction of
403 the A-P body axis, and did not further analyze the stimulus data of the D-V
404 body axis. We have observed that most of hair cells that responded to the flow
405 from the direction P to A were more active than that from A to P (Fig5 J; sample,
406 Fig5 C,D) and that those responded to the opposite flow came in pairs(Fig 5 I).
407 All these suggest that it looks like being arranged beforehand rather than at
408 random though only a part of cells in one neuromast responded to flow
409 stimulation.

410 In summary, our research suggests that suppression of inflammation
411 delays functional regeneration of lateral hair cells in zebrafish larvae. The
412 inflammation plays positive and permissive roles in regeneration of hair cells.

413

414 Materials and Methods

415 Zebrafish strains and maintenance

416 AB/Wild-type strain, Tg(corola-eGFP;lyz-Dsred) and Huc:h2b-gcamp6f
417 transgenic line were used in this study. Embryos were generated by paired
418 mating and maintained at 28.5℃ in EM and on a 14/10 h light/dark cycle

bioRxiv preprint doi: https://doi.org/10.1101/2020.02.26.962753; this version posted February 26, 2020. The copyright holder for this preprint (which was not certified by peer review) is the author/funder, who has granted bioRxiv a license to display the preprint in perpetuity. It is made available under aCC-BY-NC-ND 4.0 International license.

419 according to the standard protocols.

420 All animal manipulations were conducted strictly in accordance with the
421 guidelines and regulations set forth by the University of Science and
422 Technology of China (USTC) Animal Resources Center and the University
423 Animal Care and Use Committee. The protocol was approved by the
424 Committee on the Ethics of Animal Experiments of the USTC (Permit Number:
425 USTCACUC1103013).

426 **Hair cell damage and inflammation inhibition**

427 In order to damage hair cells in lateral line, 4 dpf Larvae were treated with
428 5 μM $CuSO_4$(Sangon, China) diluted in embro medium (EM) for 1 h. Then, they
429 were washed three times and recovered in EM.

430 To suppress inflammation, 4 dpf larvae were immersed in 0.1% BRS-28,
431 an anti-inflammatory agent, for 3 h before being moved into $CuSO_4$ to damage
432 hair cells.

433 **Live imaging**

434 AB/Wild-type larvae were used to count the number of regenerated hair
435 cells in L2、LII2、L3 neuromasts (Fig. 1A). Hair cells were marked by
436 0.01 %DAPI for 5 minutes. Being anesthetized in 0.02% MS-222 (Tricaine
437 mesylate, Sigma,USA), larvae were imaged under a fluorescence microscope
438 (Olympus BX-60, Japan).

439 In order to exhibit the damage of hair cells in copper sulfate solution and
440 the regeneration of hair cell in different phases, hair cells were labeled by
441 0.05 % DASPEI (Sigma, USA), and larvae were anesthetized in MS-222 and
442 imaged under a confocal microscopy (Zeiss LSM 880 +Airyscan, Germany).

443 Tg(corola-eGFP; lyz-Dsred) transgenic line was used to observe the
444 number of neutrophils and macrophages migrating to the injured neuromasts
445 *in vivo*. This transgenic line expressed the enhanced green fluorescent protein
446 (eGFP) in macrophages and expressed both eGFP and Dsred in neutrophils,

bioRxiv preprint doi: https://doi.org/10.1101/2020.02.26.962753; this version posted February 26, 2020. The copyright holder for this preprint (which was not certified by peer review) is the author/funder, who has granted bioRxiv a license to display the preprint in perpetuity. It is made available under aCC-BY-NC-ND 4.0 International license.

447 which shows yellow fluorescent when merged. To show the neutrophils and
448 macrophages migrating to damaged neuromasts, larvae were anesthetized in
449 MS-222 and imaged under a confocal microscopy (Zeiss LSM 880 +Airyscan).
450 For neutrophils and macrophages counting, we determined the area within 100
451 μm around the L2、LII2、L3 neuromasts as the target. Zebrafish larvae were
452 anesthetized and imaged by the fluorescence microscope (Olympus BX-60)
453 with a green and a red channel.

454 **Rheotaxis behavior experiments**

455 A U-shaped tank was designed to test the rheotaxis behavior of larvae
456 (Fig 4A). The bottom of the two cubic tanks (7 cm length *8 cm width*8 cm
457 height) were connected by a platform (10 cm length *8 cm width*0.5 cm height).
458 A peristaltic pump (Longer Pump YZ1515x,China) was used to move EM
459 solution from the left tank to the right one, so that, a stable reverse flow was
460 formed (right to left, v=10 mm/s). AB/WT zebrafish larvae were applied to
461 detect the ability of rheotaxis. Larvae were released at the right side of the
462 platform with early velocity almost equals 0. To avoid visual cues, experiments
463 were operated in the dark and rheotaxis performs were recorded by an infrared
464 CCD (IR850, weixinshijie, China).

465 Rheotaxis data were analyzed by our own rheotaxis software edited in
466 Matlab (2015a, MathWorks, USA). This software can plot the movement track
467 of zebrafish larvae in the platform, measure the direction and distance of each
468 swimming and calculate the speed of each movement. Finally, it reports scores
469 based on the magnitude in the horizontal direction of the ratio of motion
470 vectors sum to the motion arithmetic sum.

471 **Calcium imaging and data analyses**

472 Huc: h2b-GCamp6f transgenic line was used in calcium imaging which
473 expressed pan-neuronal nucleus-labelled GCamp6f. Larvae were
474 anesthetized and fixed by a net pressure. The one-step pulled micropipette

bioRxiv preprint doi: https://doi.org/10.1101/2020.02.26.962753; this version posted February 26, 2020. The copyright holder for this preprint (which was not certified by peer review) is the author/funder, who has granted bioRxiv a license to display the preprint in perpetuity. It is made available under aCC-BY-NC-ND 4.0 International license.

475 had a long, wispy tip which must be trimmed by rubbing it against with another
476 pulled micropipette to generate a tip with an outer diameter of approximately
477 40 μm. The micropipette was filled with MS-222 and fixed to the holder of a
478 micromanipulator (MX7500, Scientific Design Company, USA). The tip of the
479 micropipette should be positioned at a distance of approximately 100 μm from
480 the top of the kinocilia (Fig.5 A). The duration of flow was controlled by
481 three direct links which were linked with a syringe.

482 Calcium imaging was collected by a confocal microscopy (FV 1000,
483 Olympus, Japan). In order to make as many hair cells as possible in the
484 observation area at the same time, a single z-axis was adjusted. Region of
485 interest (ROI) was set to 110*108. We took 100 time-lapse images for each
486 neuromast, and the total capture time was 29.7 s (0.297 s per slice). Flow
487 stimulation occured at the period from 10.098 to 19.899 s.

488 Since the neuromasts are three-dimensional, different hair cells have
489 different levels of fluorescence intensity. Namely, they have different levels of F
490 prime. The relative fluorescence intensity change ($\Delta F/F_0$) is more commonly
491 used. For each hair cell, the average fluorescence intensity before flow stimuli
492 (0-10 s) was set as F_0. The data would be excluded when F_0<95, which means
493 these hair cells were too far from the focal plane. If neuromasts had more than
494 two hair cells that responded to the flow stimulus, we took only the two that
495 responded the most in the fluorescence intensity change curve.

496 **Statistical analysis**

497 All data were shown as mean ± S.E.M. or as relative proportions of 100 % as
498 indicated in the appropriate legends. The data were analyzed in either
499 one-way ANOVA with Tukey's multiple comparisons test or two-way ANOVA
500 with Tukey's multiple comparisons test by GraphPad Prism version 7.0 (Prism,
501 San Diego, CA, USA). The level of significance was set to P < 0.05. *, **and
502 ***represent P < 0.05, P < 0.01 and P < 0.001, respectively.

bioRxiv preprint doi: https://doi.org/10.1101/2020.02.26.962753; this version posted February 26, 2020. The copyright holder for this preprint (which was not certified by peer review) is the author/funder, who has granted bioRxiv a license to display the preprint in perpetuity. It is made available under aCC-BY-NC-ND 4.0 International license.

503

504 ## Acknowledgments

505 The authors thank Drs. Wen Zilong for providing the Tg(corola-eGFP;
506 lyz-Dsred) transgenic fish line, Drs. Wen Quan for providing the
507 Huc:h2b-gcamp6f transgenic fish line. The authors thank Drs. Zhen Xuechu for
508 providing BRS-28 and the compound-26 in their study is the BRS-28
509 mentioned in this study.

510

511 ## References

512 **Aman, A., and Piotrowski, T. (2008). Wnt/beta-catenin and Fgf signaling control
513 collective cell migration by restricting chemokine receptor expression. Developmental
514 cell *15*, 749-761.**
515 **Baird, R.A., Steyger, P.S., and Schuff, N.R. (1996). Mitotic and nonmitotic hair cell
516 regeneration in the bullfrog vestibular otolith organs. Annals of the New York Academy
517 of Sciences *781*, 59-70.**
518 **Carrillo, S.A., Anguita-Salinas, C., Pena, O.A., Morales, R.A., Munoz-Sanchez, S.,
519 Munoz-Montecinos, C., Paredes-Zuniga, S., Tapia, K., and Allende, M.L. (2016).
520 Macrophage Recruitment Contributes to Regeneration of Mechanosensory Hair Cells in
521 the Zebrafish Lateral Line. Journal of cellular biochemistry *117*, 1880-1889.**
522 **Chai, R., Kuo, B., Wang, T., Liaw, E.J., Xia, A., Jan, T.A., Liu, Z., Taketo, M.M., Oghalai,
523 J.S., Nusse, R.*, et al.* (2012). Wnt signaling induces proliferation of sensory precursors
524 in the postnatal mouse cochlea. Proceedings of the National Academy of Sciences of
525 the United States of America *109*, 8167-8172.**
526 **Chou, S.W., Chen, Z., Zhu, S., Davis, R.W., Hu, J., Liu, L., Fernando, C.A., Kindig, K.,
527 Brown, W.C., Stepanyan, R.*, et al.* (2017). A molecular basis for water motion detection
528 by the mechanosensory lateral line of zebrafish. Nature communications *8*, 2234.**
529 **Coombs., S., Bleckmann., H., Fay., R.R., and Popper, A.N. (2014). The Lateral Line
530 System (New York: Springer).**
531 **Dijkgraaf, S. (1962). The functioning and significance of the lateral-line organs.
532 Biological Reviews of the Cambridge Philosophical Society *38: 51-105*.**
533 **Fan, Y., and Bergmann, A. (2008). Apoptosis-induced compensatory proliferation.
534 The Cell is dead. Long live the Cell! Trends in cell biology *18*, 467-473.**
535 **Flock, A., and Wersall, J. (1962). A study of the orientation of the sensory hairs of
536 the receptor cells in the lateral line organ of fish, with special reference to the function
537 of the receptors. The Journal of cell biology *15*, 19-27.**
538 **Kniss, J.S., Jiang, L., and Piotrowski, T. (2016). Insights into sensory hair cell**

bioRxiv preprint doi: https://doi.org/10.1101/2020.02.26.962753; this version posted February 26, 2020. The copyright holder for this preprint (which was not certified by peer review) is the author/funder, who has granted bioRxiv a license to display the preprint in perpetuity. It is made available under aCC-BY-NC-ND 4.0 International license.

539 **regeneration from the zebrafish lateral line. Current opinion in genetics & development**
540 ***40*, 32-40.**
541 **Kurimoto, T., Yin, Y., Habboub, G., Gilbert, H.Y., Li, Y., Nakao, S., Hafezi-Moghadam,**
542 **A., and Benowitz, L.I. (2013). Neutrophils express oncomodulin and promote optic**
543 **nerve regeneration. The Journal of neuroscience : the official journal of the Society for**
544 **Neuroscience *33*, 14816-14824.**
545 **Li, L., Yan, B., Shi, Y.Q., Zhang, W.Q., and Wen, Z.L. (2012). Live imaging reveals**
546 **differing roles of macrophages and neutrophils during zebrafish tail fin regeneration.**
547 **The Journal of biological chemistry *287*, 25353-25360.**
548 **Lopez-Schier, H., and Hudspeth, A.J. (2006). A two-step mechanism underlies the**
549 **planar polarization of regenerating sensory hair cells. Proceedings of the National**
550 **Academy of Sciences of the United States of America *103*, 18615-18620.**
551 **Lush, M.E., and Piotrowski, T. (2014). Sensory hair cell regeneration in the zebrafish**
552 **lateral line. Developmental dynamics : an official publication of the American**
553 **Association of Anatomists *243*, 1187-1202.**
554 **Ma, E.Y., Rubel, E.W., and Raible, D.W. (2008). Notch signaling regulates the extent**
555 **of hair cell regeneration in the zebrafish lateral line. The Journal of neuroscience : the**
556 **official journal of the Society for Neuroscience *28*, 2261-2273.**
557 **Matsui., J.I., and Cotanchea., D.A. (2004). Sensory hair cell death and regeneration**
558 **two halves of the same equation. Hearing Science.**
559 **Mescher, A.L. (2017). Macrophages and fibroblasts during inflammation and tissue**
560 **repair in models of organ regeneration. Regeneration *4*, 39-53.**
561 **Mizutari, K., Fujioka, M., Hosoya, M., Bramhall, N., Okano, H.J., Okano, H., and Edge,**
562 **A.S. (2013). Notch inhibition induces cochlear hair cell regeneration and recovery of**
563 **hearing after acoustic trauma. Neuron *77*, 58-69.**
564 **Mollereau, B., Perez-Garijo, A., Bergmann, A., Miura, M., Gerlitz, O., Ryoo, H.D.,**
565 **Steller, H., and Morata, G. (2013). Compensatory proliferation and apoptosis-induced**
566 **proliferation: a need for clarification. Cell death and differentiation *20*, 181.**
567 **Nechiporuk, A., and Raible, D.W. (2008). FGF-Dependent Mechanosensory Organ**
568 **Patterning in Zebrafish. Science *320*, 1774-1777.**
569 **Oesterle, E.C., and Stone, J.S. (2008). Hair Cell Regeneration: Mechanisms Guiding**
570 **Cellular Proliferation and Differentiation. In Hair Cell Regeneration, Repair and**
571 **Protection, RJ Salvi , A. Popper, and R. Fay, eds. (New York: Springer), pp. 141-197.**
572 **Olszewski, J., Haehnel, M., Taguchi, M., and Liao, J.C. (2012). Zebrafish Larvae**
573 **Exhibit Rheotaxis and Can Escape a Continuous Suction Source Using Their Lateral**
574 **Line. PloS one *7*, e36661.**
575 **Pereira, T.C., Campos, M.M., and Bogo, M.R. (2016). Copper toxicology, oxidative**
576 **stress and inflammation using zebrafish as experimental model. Journal of applied**
577 **toxicology : JAT *36*, 876-885.**
578 **Popper, A.N., and Hoxter, B. (1984). Growth of a fish ear: 1. Quantitative analysis of**
579 **hair cell and ganglion cell proliferation. Hearing research *15*, 133-142.**
580 **Raphael, Y. (1992). Evidence for supporting cell mitosis in response to acoustic**

bioRxiv preprint doi: https://doi.org/10.1101/2020.02.26.962753; this version posted February 26, 2020. The copyright holder for this preprint (which was not certified by peer review) is the author/funder, who has granted bioRxiv a license to display the preprint in perpetuity. It is made available under aCC-BY-NC-ND 4.0 International license.

581 **trauma in the avian inner ear. J Neurocytol *21*, 663-671.**
582 **Renshaw, S.A., and Trede, N.S. (2012). A model 450 million years in the making:**
583 **zebrafish and vertebrate immunity. Disease models & mechanisms *5*, 38-47.**
584 **Roberson, D.W., Alosi, J.A., and Cotanche, D.A. (2004). Direct transdifferentiation**
585 **gives rise to the earliest new hair cells in regenerating avian auditory epithelium.**
586 **Journal of Neuroscience Research *78*, 461-471.**
587 **Romero-Carvajal, A., Navajas Acedo, J., Jiang, L., Kozlovskaja-Gumbriene, A.,**
588 **Alexander, R., Li, H., and Piotrowski, T. (2015). Regeneration of Sensory Hair Cells**
589 **Requires Localized Interactions between the Notch and Wnt Pathways. Developmental**
590 **cell *34*, 267-282.**
591 **Rubbini, D., Robert-Moreno, A., Hoijman, E., and Alsina, B. (2015). Retinoic Acid**
592 **Signaling Mediates Hair Cell Regeneration by Repressing p27kip and sox2 in**
593 **Supporting Cells. The Journal of neuroscience : the official journal of the Society for**
594 **Neuroscience *35*, 15752-15766.**
595 **Shimizu, N., Kawakami, K., and Ishitani, T. (2012). Visualization and exploration of**
596 **Tcf/Lef function using a highly responsive Wnt/β-catenin signaling-reporter transgenic**
597 **zebrafish. Developmental Biology *370*, 71-85.**
598 **Stone., J.S., and Rubel., E.W. (2000). Cellular studies of auditory hair cell**
599 **regeneration in birds. PNAS.**
600 **Suli, A., Watson, G.M., Rubel, E.W., and Raible, D.W. (2012). Rheotaxis in Larval**
601 **Zebrafish Is Mediated by Lateral Line Mechanosensory Hair Cells. PloS one *7*, e29727.**
602 **Thomas, E.D., Cruz, I.A., Hailey, D.W., and Raible, D.W. (2015). There and back again:**
603 **development and regeneration of the zebrafish lateral line system. Wiley Interdiscip Rev**
604 **Dev Biol *4*, 1-16.**
605 **Tian, L., Hires, S.A., and Looger, L.L. (2012). Imaging neuronal activity with**
606 **genetically encoded calcium indicators. Cold Spring Harbor protocols *2012*, 647-656.**
607 **Yang, Y.X., Zheng, L.T., Shi, J.J., Gao, B., Chen, Y.K., Yang, H.C., Chen, H.L., Li, Y.C.,**
608 **and Zhen, X.C. (2014). Synthesis of 5alpha-cholestan-6-one derivatives and their**
609 **inhibitory activities of NO production in activated microglia: discovery of a novel**
610 **neuroinflammation inhibitor. Bioorganic & medicinal chemistry letters *24*, 1222-1227.**
611 **Yorgason., J.G., Fayad., J.N., and Kalinec., F. (2006). Understanding drug ototoxicity:**
612 **molecular insights for preventionand clinical management. Biological Reviews.**
613 **Zhang, Q., Li, S., Wong, H.C., He, X.J., Beirl, A., Petralia, R.S., Wang, Y.X., and Kindt,**
614 **K.S. (2018). Synaptically silent sensory hair cells in zebrafish are recruited after damage.**
615 **Nature communications *9*, 1388.**
616 **Zhang, Q.X., He, X.J., Wong, H.C., and Kindt, K.S. (2016). Functional calcium**
617 **imaging in zebrafish lateral-line hair cells. Methods in cell biology *133*, 229-252.**
618

619

620

bioRxiv preprint doi: https://doi.org/10.1101/2020.02.26.962753; this version posted February 26, 2020. The copyright holder for this preprint (which was not certified by peer review) is the author/funder, who has granted bioRxiv a license to display the preprint in perpetuity. It is made available under aCC-BY-NC-ND 4.0 International license.

621 **Fig. 1 $CuSO_4$ damaged hair cells in lateral line of zebrafish.**

622 **(A)** Lateral line hair cells in a 6 day post fertilization (dpf) AB/WT zebrafish
623 larvae are labeled with 0.05% DASPEI. L2, LII3 and L3 neuromasts are
624 marked with circles. Scale bar represents 500 μm.

625 **(B)** Lateral view of a neuromast shows sensory hair cells in the center labeled
626 with DASPEI and a bundle of kinocilia (arrow) extend out of the periderm.
627 Scale bar represents 50 μm.

628 **(C)** A cartoon illustrating the structure of the neuromast.

629 **(D)**Time lapse imaging shows that when merged in 5 μM $CuSO_4$ solution, hair
630 cells were gradually injured and damaged within 60 min. Scale bar
631 represents 10 μm.

632 **(E)** DASPEI staining displays that hair cells regenerate completely within
633 96 hours post injured (hpi). Scale bar represents 10 μm.

634

bioRxiv preprint doi: https://doi.org/10.1101/2020.02.26.962753; this version posted February 26, 2020. The copyright holder for this preprint (which was not certified by peer review) is the author/funder, who has granted bioRxiv a license to display the preprint in perpetuity. It is made available under aCC-BY-NC-ND 4.0 International license.

635
636
637 **Fig. 2 BRS-28 reduces the number of neutrophils and macrophages**
638 **migrating to the injured neuromasts.**
639 **(A-C)** Live imaging (×40) displays the regions of L3 neuromasts of larvae
640 at GFP channel, Dsred channel, and bright field (BF) channel and
641 superimposed image in different group. Neutrophils (show both green and
642 yellow fluorescence, indicated by white arrows) and macrophages (show olny
643 green fluorescence, indicated by blue arrows) around the neuromasts can be
644 observed in Tg(corola-eGFP; lyz-Dsred) larvae. They are almost absent from
645 the neuromasts in control **(A)**. Many neutrophils and macrophages migrate to
646 injured neuromasts in $CuSO_4$ group **(B)** while fewer neutrophils and
647 macrophages migrate to injured neuromasts in BRS+$CuSO_4$ group **(C)**. The
648 image is captured after adding $CuSO_4$ solution for 1 h. Scale bar represents 50
649 μm.
650 **(D-E)** Line charts reveal decreased numbers of neutrophils **(D)** and
651 macrophages **(E)** within a radius of 50 μm from the center of neuromasts at
652 different time points after adding $CuSO_4$ in BRS+$CuSO_4$ group ($n \geq 16$) than
653 $CuSO_4$ group ($n \geq 15$). Control ($n \geq 11$) is observed at the same time points.
654 To **(D)** and **(E)**, comparisons were performed by using two-way ANOVA,
655 with Tukey's multiple comparisons test. All Error bars show mean ± S.E.M., ***
656 $P < 0.001$, **$P < 0.01$,*$P < 0.05$.
657
658

bioRxiv preprint doi: https://doi.org/10.1101/2020.02.26.962753; this version posted February 26, 2020. The copyright holder for this preprint (which was not certified by peer review) is the author/funder, who has granted bioRxiv a license to display the preprint in perpetuity. It is made available under aCC-BY-NC-ND 4.0 International license.

659

660 **Fig. 3 Suppressing inflammation delays hair cell regeneration.**

661 **(A)** Real-time imaging (×40) displays regenerated hair cells in the $CuSO_4$
662 and BRS+$CuSO_4$ group at 24, 48 and 96 hpi. Control group is taken at the
663 same time point. Scale bar represents 10 μm.

664 **(B)** The numbers of regenerated hair cells were significantly decreased in
665 BRS+$CuSO_4$ group than that in $CuSO_4$ group at 16 (P=0.0061), 24 (P=0.0021)
666 and 48(P<0.0001) hpi. At 96 hpi, hair cells in both $CuSO_4$ group and
667 BRS+$CuSO_4$ group regenerated to normal levels.

668 Linear analysis in $CuSO_4$ group **(C)** and BRS+$CuSO_4$ group **(D)** were
669 conducted on the number of regeneration within 48 hours. The slope in $CuSO_4$
670 group (0.1879) is higher than that in BRS+$CuSO_4$ group (0.148) and
671 x-intercept in $CuSO_4$ group (4.16) is higher than that in BRS+CuSO4 group
672 (8.287).

673 **(E)** When delay the time window of inflammatory suppression, there is no
674 delay in the regeneration of hair cells. BRS-28 was added at the same time as
675 $CuSO_4$ ($CuSO_4$+BRS 0 h group), or 30 minutes after the addition of $CuSO_4$
676 ($CuSO_4$+BRS 0.5 h group), or 1 hour after the addition of $CuSO_4$ ($CuSO_4$+BRS
677 1 h group)(n≥27 neuromasts in each time point of each group).

678 To **(B)** and **(E)**, comparisons were performed by using two-way ANOVA,
679 with Tukey's multiple comparisons test. All Error bars show mean ± S.E.M., ***
680 P < 0.001, **P < 0.01,*P < 0.05.

681

bioRxiv preprint doi: https://doi.org/10.1101/2020.02.26.962753; this version posted February 26, 2020. The copyright holder for this preprint (which was not certified by peer review) is the author/funder, who has granted bioRxiv a license to display the preprint in perpetuity. It is made available under aCC-BY-NC-ND 4.0 International license.

682

683 **Fig.4 The recovery of the functional of lateral line system was**
684 **delayed when inflammation was suppressed.**

685 **(A)** A U-shaped tank was designed to test the rheotaxis behavior of larvae.
686 A peristaltic pump was used to form flow at the bottom of the tank. Larvae were
687 placed from the right platform, and they sense the water flow from right to left.
688 Rheotaxis perform was recorded by an infrared CCD.

689 A larva with excellent rheotaxis **(B)** and a larva with poor rheotaxis **(C)**
690 were analyzed by behavioral analysis software. Moving traces were plotted in
691 left panels and the motion vector were displayed in right panels. The lengths of
692 the blue segments represented the distance of each movement, and the
693 direction of the blue segment represented the direction of that movement. The
694 length of the red line segment was the ratio of motion vectors sum to the
695 motion arithmetic sum and the direction was the direction of the sum of the
696 vectors.

697 **(D)** Rheotaxis score revealed that at 24 and 48 hpi, the rheotaxis of
698 BRS+$CuSO_4$ group was significantly lower than that of control. On the contrary,
699 the rheotaxis of $CuSO_4$ group was not significantly different from that of control
700 within 24 hpi.

701 The speed **(E)** and distance **(F)** of larvae swimming at each time were
702 consistent within different times and between different groups.

703 To **(D-F)**, comparisons were performed by using two-way ANOVA, with
704 Tukey's multiple comparisons test. All Error bars show mean ± S.E.M., $^{**}P <$
705 0.01,$^{*}P < 0.05$.

706

707

bioRxiv preprint doi: https://doi.org/10.1101/2020.02.26.962753; this version posted February 26, 2020. The copyright holder for this preprint (which was not certified by peer review) is the author/funder, who has granted bioRxiv a license to display the preprint in perpetuity. It is made available under aCC-BY-NC-ND 4.0 International license.

708

709 **Fig.5 Calcium imaging revealed the function of a single neuromast**
710 **after hair cell regeneration**

711 **(A)** Schematic diagram shows an electrode filled with fluid is located about
712 100 μm away from the top of kinocilia to stimulate the neuromast. The yellow
713 and green hair cells represent different polarities.

714 **(B)** When stimulated by the flow, only a part of hair cells respond in this
715 focal plane (circled cells), and some are far from this focal plane (dashed
716 circled cells). The No. 2, 4, and 6 active hair cells (yellow circles) only respond
717 to the flow in P-A direction **(C)**. At the same time, the No. 1, 3, and 5 active hair
718 cells (green circles) only respond to the flow in A-P direction **(D).** Scale bar in
719 **(B)** represents 10 μm.

720 **(E)** The fluorescence intensity (ΔF/F) of the BRS + $CuSO_4$ group is
721 significantly lower than that of the $CuSO_4$ group in the Early Stage of
722 regeneration (within 48 hpi)($P < 0.001$).

723 **(F)** The ΔF/F of BRS+$CuSO_4$ group is not significantly different from that
724 of control group and $CuSO_4$ group in the Late Stage of regeneration (72-96
725 hpi)

726 **(G)** There is no difference in ΔF/F between the BRS group and the control
727 group.

728 **(H)** During the regeneration process, the number of active hair cells in
729 $CuSO_4$ and BRS+$CuSO_4$ group is basically the same, and did not increase
730 with the total number of regenerated hair cells.

731 To **(E-H)**, comparisons were performed by using one-way ANOVA, with
732 Tukey's multiple comparisons test.

733

734

735

bioRxiv preprint doi: https://doi.org/10.1101/2020.02.26.962753; this version posted February 26, 2020. The copyright holder for this preprint (which was not certified by peer review) is the author/funder, who has granted bioRxiv a license to display the preprint in perpetuity. It is made available under aCC-BY-NC-ND 4.0 International license.

736

737 **Supplementary Fig. 1 $CuSO_4$ caused apoptosis in hair cells.**

738

739 TUNEL assay revealed hair cells occurred apoptosis when treated with

740 $CuSO_4$. Nuclei were stained with DAPI. BF: Bright Field. Scale bar represents 20 μm.

741

742

bioRxiv preprint doi: https://doi.org/10.1101/2020.02.26.962753; this version posted February 26, 2020. The copyright holder for this preprint (which was not certified by peer review) is the author/funder, who has granted bioRxiv a license to display the preprint in perpetuity. It is made available under aCC-BY-NC-ND 4.0 International license.

743
744 **Supplementary Fig. 2 Tg(corola-eGFP; lyz-Dsred) transgenic line**
745 **could mark both neutrophils and macrophages.**
746
747 This transgenic line expresses the enhanced green fluorescent protein
748 (eGFP) in macrophages and expresses both eGFP and the enhanced red
749 fluorescent protein (DsRed) in neutrophils, which shows yellow fluorescent
when merged. Scale bar represents 200 μm.

750
751
752

bioRxiv preprint doi: https://doi.org/10.1101/2020.02.26.962753; this version posted February 26, 2020. The copyright holder for this preprint (which was not certified by peer review) is the author/funder, who has granted bioRxiv a license to display the preprint in perpetuity. It is made available under aCC-BY-NC-ND 4.0 International license.

753

754 **Supplementary Fig. 3 Most active hair cells are polar in pairs and are**
755 **sensitive to flow in the P-A direction.**
756
757 **(A)** Most hair cells that responded to the flow in the opposite direction
758 come in pairs.
759 **(B)** The fluorescence intensity of hair cells responding to P-A direction is significantly higher than that of hair cells responding to A-P direction.

760 To **(A,B)**, comparisons were performed by using one-way ANOVA, with
761 Tukey's multiple comparisons test. All Error bars show mean ± S.E.M.
762

763

764

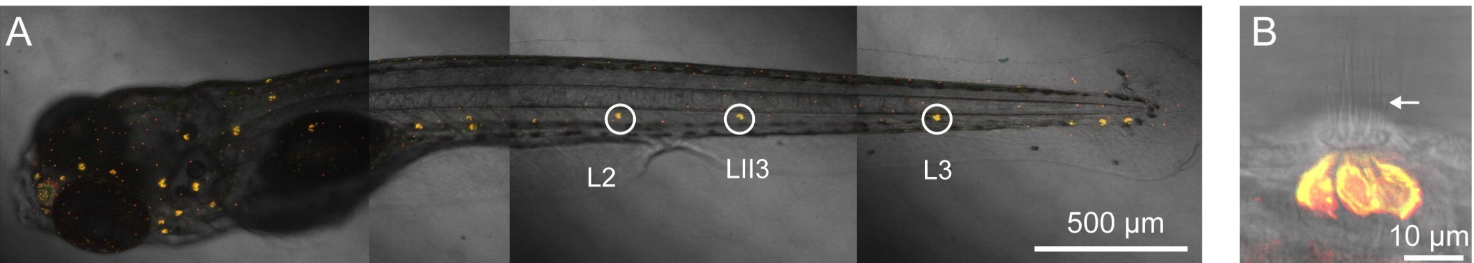
A
L2
LII3
L3
500 µm
B
10 µm

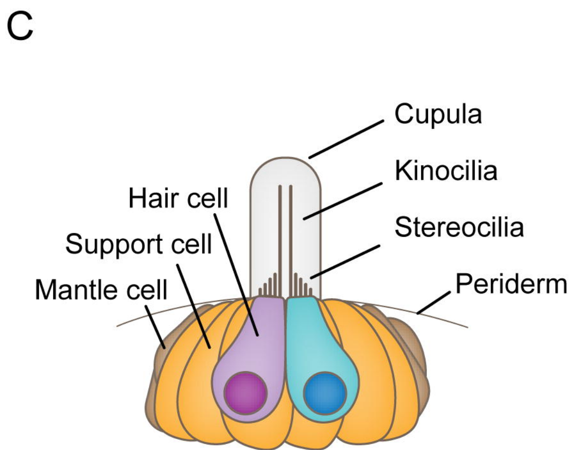
C
Cupula
Kinocilia
Hair cell
Stereocilia
Support cell
Mantle cell
Periderm

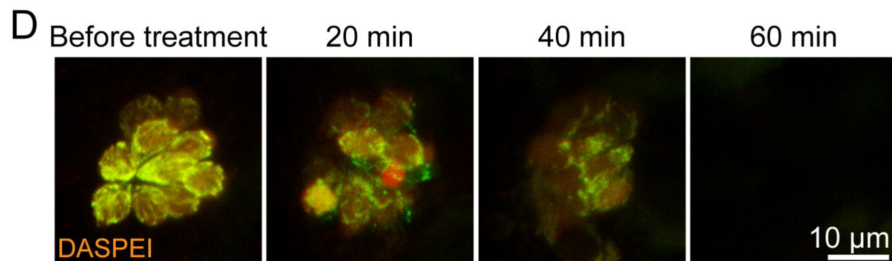
D
Before treatment
20 min
40 min
60 min
DASPEI
10 µm

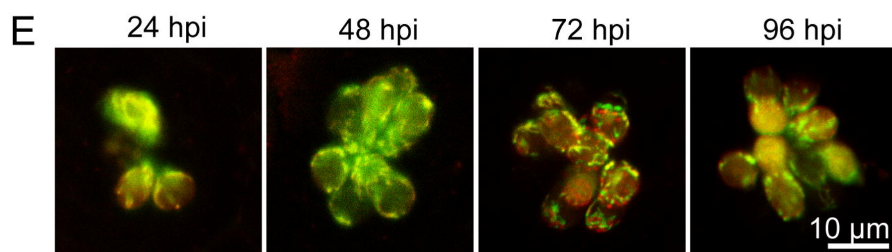
E
24 hpi
48 hpi
72 hpi
96 hpi
10 µm

	eGPF	Dsred	BF	Merge
A Control				
B $CuSO_4$				
C BRS+$CuSO_4$				50 μm

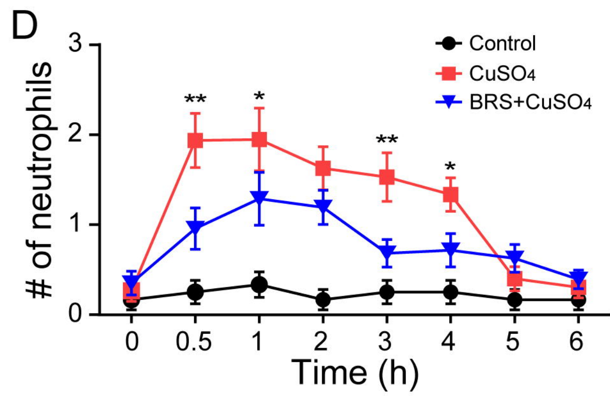

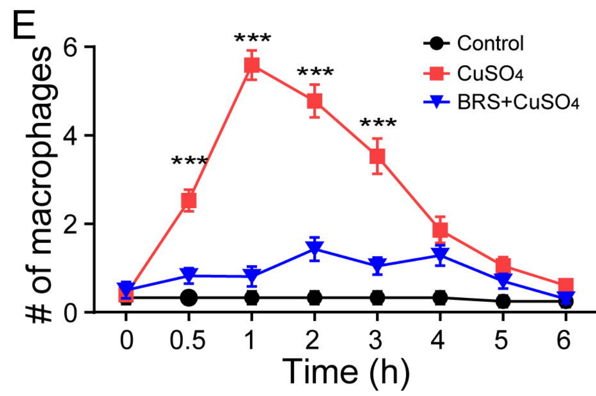

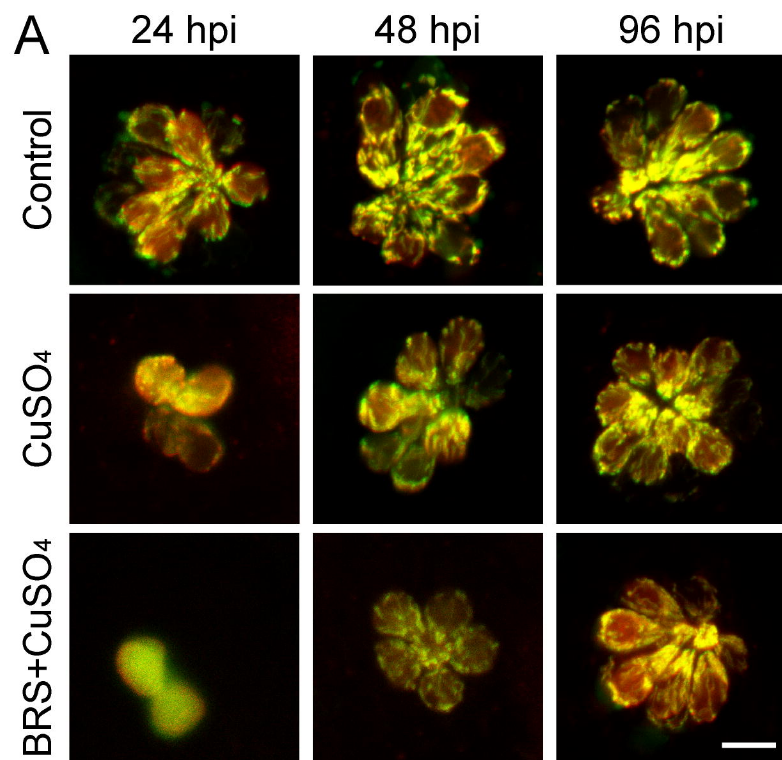
A
24 hpi
48 hpi
96 hpi
Control
CuSO4
BRS+CuSO4

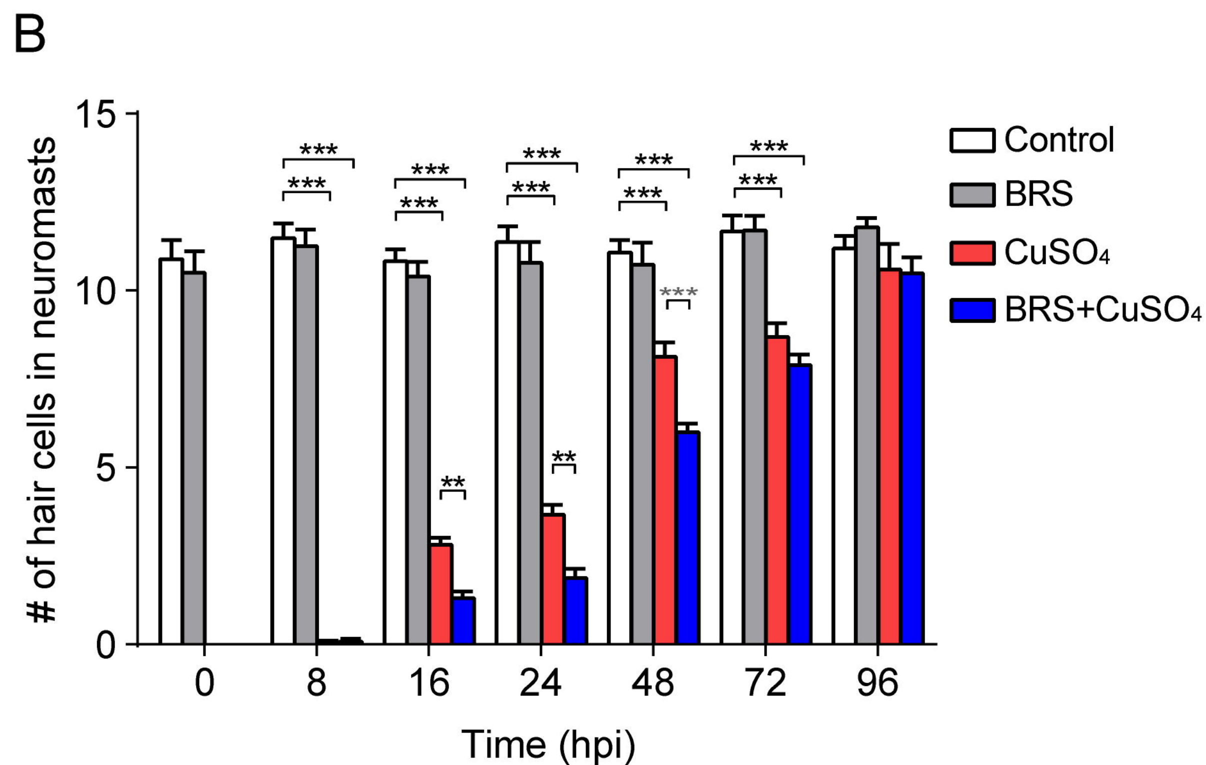
B
# of hair cells in neuromasts
Time (hpi)
Control
BRS
CuSO4
BRS+CuSO4
***
**

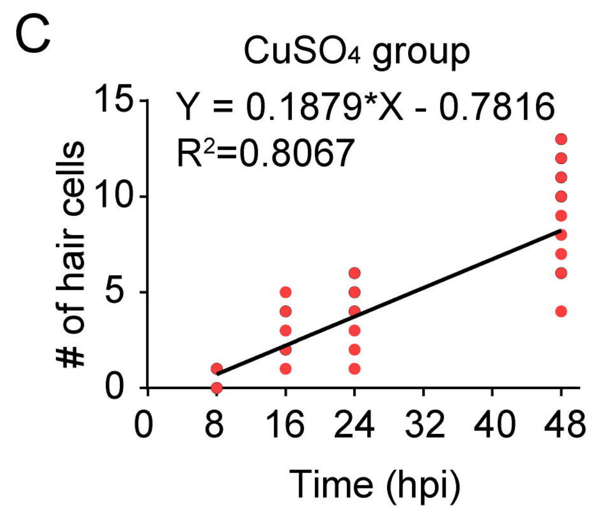
C
CuSO4 group
Y = 0.1879*X - 0.7816
R2=0.8067
# of hair cells
Time (hpi)

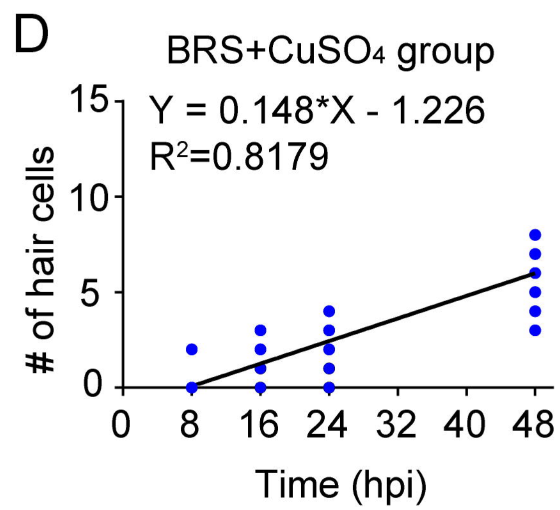
D
BRS+CuSO4 group
Y = 0.148*X - 1.226
R2=0.8179
# of hair cells
Time (hpi)

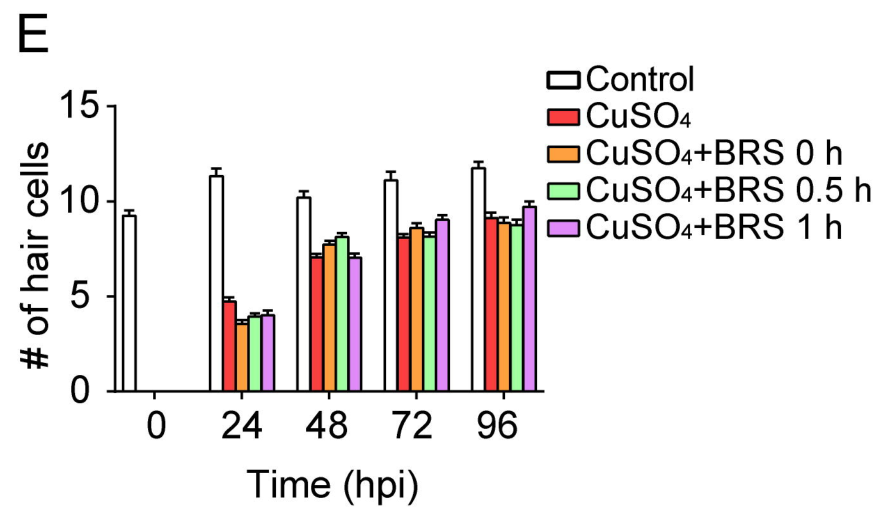
E
Control
CuSO4
CuSO4+BRS 0 h
CuSO4+BRS 0.5 h
CuSO4+BRS 1 h
# of hair cells
Time (hpi)

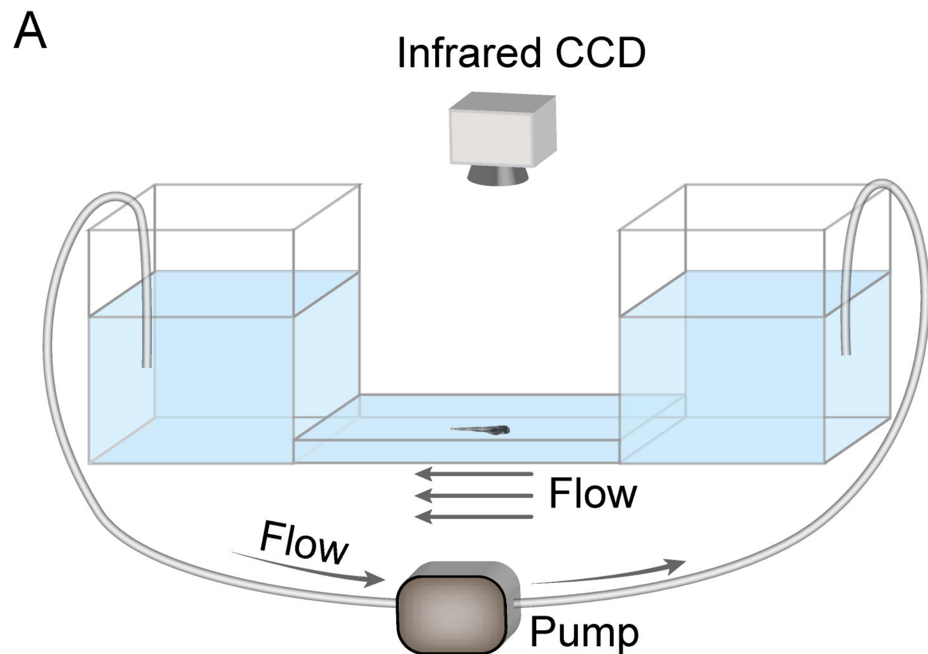
A
Infrared CCD
Flow
Flow
Pump

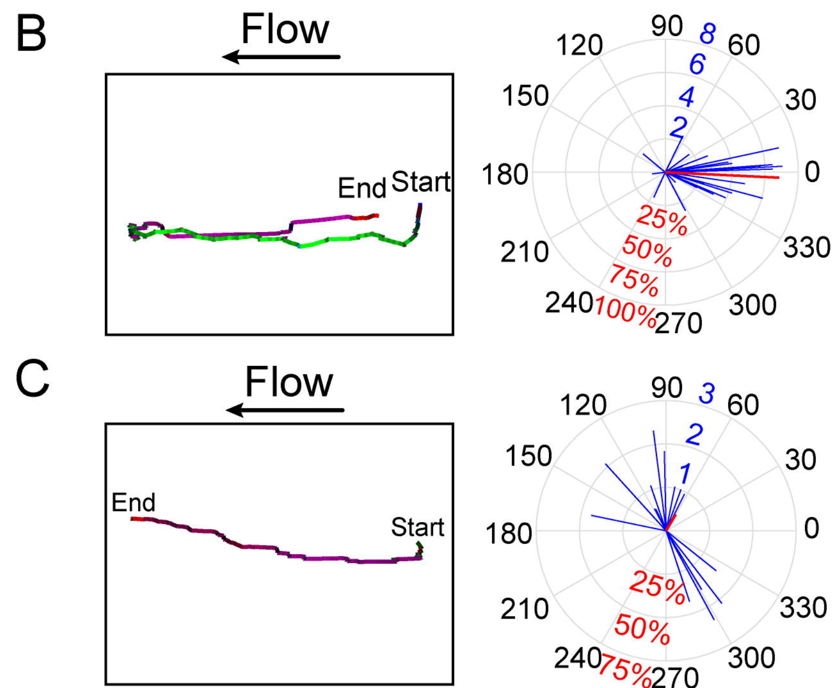
B
Flow
End
Start
C
Flow
End
Start

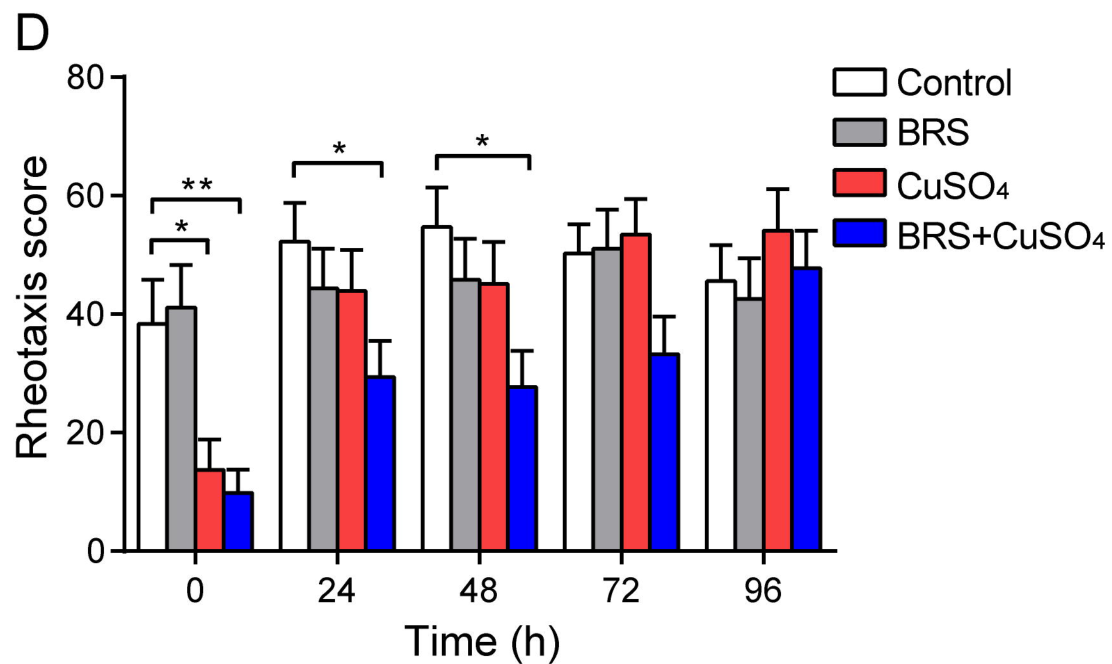
D
Rheotaxis score
Time (h)
Control
BRS
CuSO4
BRS+CuSO4

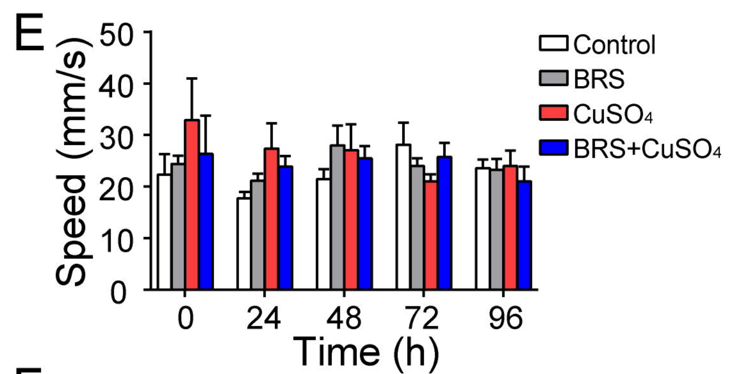
E
Speed (mm/s)
Time (h)
Control
BRS
CuSO4
BRS+CuSO4

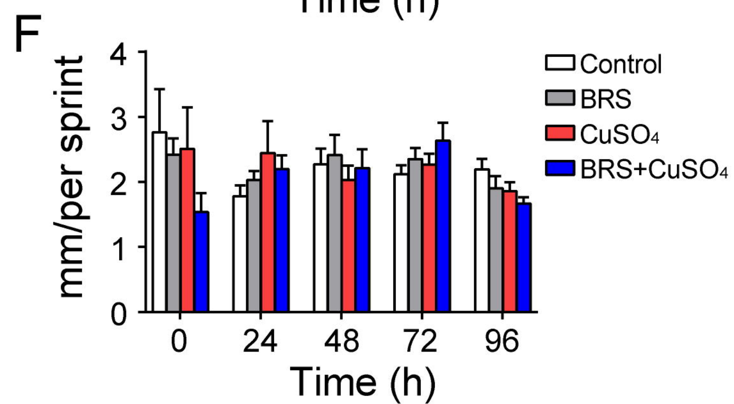
F
mm/per sprint
Time (h)
Control
BRS
CuSO4
BRS+CuSO4

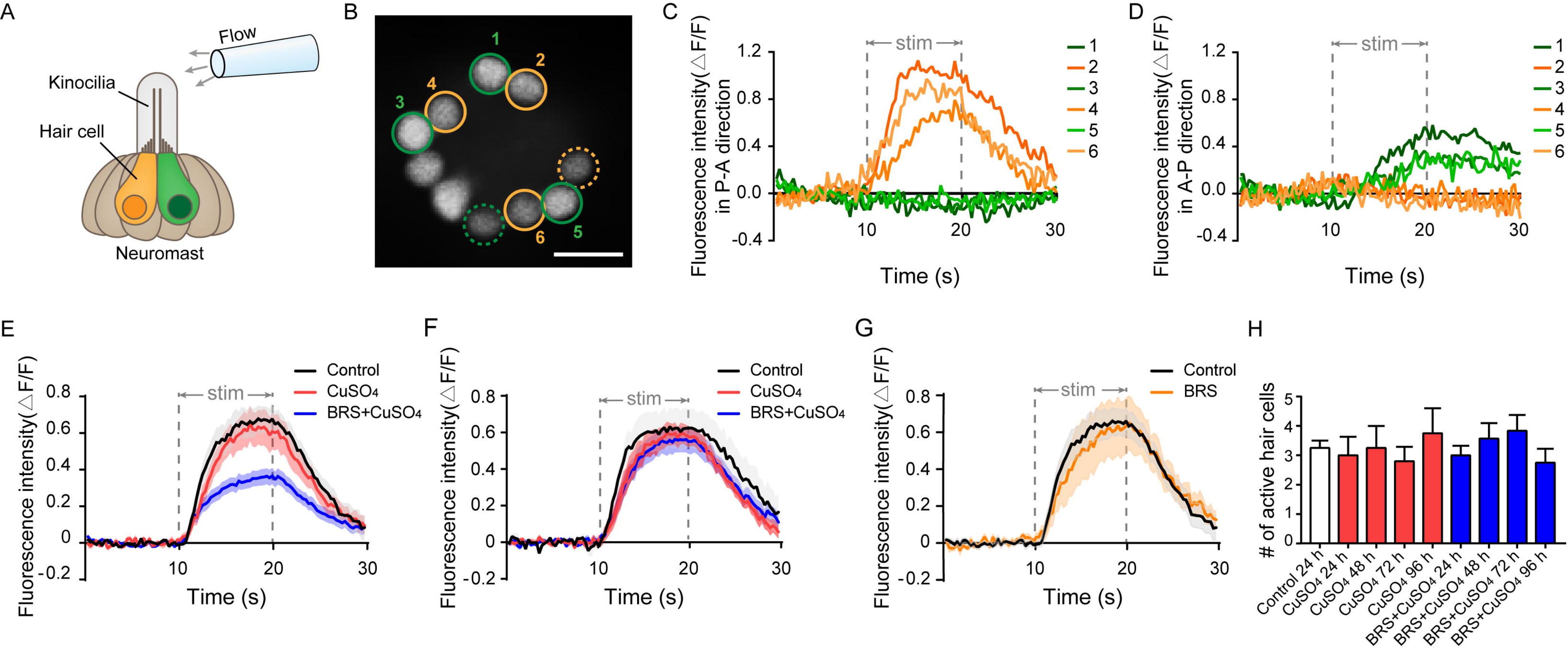
A
Flow
Kinocilia
Hair cell
Neuromast
B
C
Fluorescence intensity(△F/F) in P-A direction
stim
Time (s)
D
Fluorescence intensity(△F/F) in A-P direction
stim
Time (s)
E
Fluorescence intensity(△F/F)
Control
CuSO4
BRS+CuSO4
stim
Time (s)
F
Fluorescence intensity(△F/F)
Control
CuSO4
BRS+CuSO4
stim
Time (s)
G
Fluorescence intensity(△F/F)
Control
BRS
stim
Time (s)
H
# of active hair cells
Control 24 h
CuSO4 24 h
CuSO4 48 h
CuSO4 72 h
CuSO4 96 h
BRS+CuSO4 24 h
BRS+CuSO4 48 h
BRS+CuSO4 72 h
BRS+CuSO4 96 h